THE JOURNAL OF BIOLOGICAL CHEMISTRY VOL. 284, NO. 35, pp. 23780–23792, August 28, 2009
© 2009 by The American Society for Biochemistry and Molecular Biology, Inc. Printed in the U.S.A.

β1 Integrin Deficiency Results in Multiple Abnormalities of the Knee Joint*

Received for publication, June 30, 2009 Published, JBC Papers in Press, July 7, 2009, DOI 10.1074/jbc.M109.039347

Aurelia Raducanu[‡], **Ernst B. Hunziker**[§], **Inga Drosse**[¶], **and Attila Aszódi**[‡1]

From the [‡]*Department of Molecular Medicine, Max Planck Institute for Biochemistry, Am Klopferspitz 18, 82152 Martinsried, Germany, the* [§]*Center of Regenerative Medicine for Skeletal Tissues, Department of Clinical Research, University of Bern, 3010 Bern, Switzerland, and* [¶]*Experimental Surgery and Regenerative Medicine, Department of Surgery, University of Munich, 80336 Munich, Germany*

The lack of β1 integrins on chondrocytes leads to severe chondrodysplasia associated with high mortality rate around birth. To assess the impact of β1 integrin-mediated cell-matrix interactions on the function of adult knee joints, we conditionally deleted the β1 integrin gene in early limb mesenchyme using the *Prx1-cre* transgene. Mutant mice developed short limbed dwarfism and had joint defects due to β1 integrin deficiency in articular regions. The articular cartilage (AC) was structurally disorganized, accompanied by accelerated terminal differentiation, altered shape, and disrupted actin cytoskeleton of the chondrocytes. Defects in chondrocyte proliferation, cytokinesis, and survival resulted in hypocellularity. However, no significant differences in cartilage erosion, in the expression of matrix-degrading proteases, or in the exposure of aggrecan and collagen II cleavage neoepitopes were observed between control and mutant AC. We found no evidence for disturbed activation of MAPKs (ERK1/2, p38, and JNK) *in vivo*. Furthermore, fibronectin fragment-stimulated ERK activation and MMP-13 expression were indistinguishable in control and mutant femoral head explants. The mutant synovium was hyperplastic and frequently underwent chondrogenic differentiation. β1-null synoviocytes showed increased proliferation and phospho-focal adhesion kinase expression. Taken together, deletion of β1 integrins in the limb bud results in multiple abnormalities of the knee joints; however, it does not accelerate AC destruction, perturb cartilage metabolism, or influence intracellular MAPK signaling pathways.

Chondrocytes of the articular cartilage (AC)[2] secrete a unique set of extracellular matrix (ECM) molecules that assemble into interactive associates composed of collagens, proteoglycans (PGs), and non-collagenous glycoproteins (1). The fibrillar collagen meshwork supplies cartilage with its tensile strength, whereas the hydrated glycosaminoglycan (GAG) chains of PGs (mainly aggrecan) generate an osmotic swelling pressure that resists compressive forces. In diarthrodial joints, the molecular composition and the physical properties of the cartilage are principal determinants for the shock-absorbing function of articular surfaces upon mechanical loading. During the development of osteoarthritis (OA), an imbalance between anabolic and catabolic processes increases the proteolysis of PGs and collagens (2, 3), which eventually leads to the mechanical weakening of the AC and culminates in its progressive destruction. Physiological and pathological remodeling of the AC ECM is primarily attributed to the activities of matrix metalloproteinases (MMPs) and a disintegrin and metalloproteinase with thrombospondin-like repeat (ADAMTS) proteases (4, 5) and is controlled by the communication between the cells and their environment.

An increasing amount of evidence suggests that interactions between chondrocytes and the ECM through the integrin family of heterodimeric (αβ) transmembrane receptors play a central role in cartilage function (6). Integrins connect the pericellular matrix to cytoskeletal and intracellular signaling complexes and modulate various cellular functions, including survival, proliferation, differentiation, and matrix assembly and metabolism (7, 8). Chondrocytes express several integrin receptors for cartilage matrix ligands, such as α1β1, α2β1, and α10β1 (for collagen II); α5β1, αvβ3, and αvβ5 (for fibronectin); and α6β1 (for laminin) (6, 9). We have previously demonstrated that $\beta1^{fl/fl}$-*Col2a1cre*$^{+}$ mice, in which the floxed β1 integrin gene ($\beta1^{fl/fl}$) was deleted using the chondrocyte-specific *Col2a1cre* transgene, display severe chondrodysplasia and a high mortality rate at birth (10). Homozygous mutant mice exhibit multiple growth plate abnormalities during endochondral bone formation, characterized by defects in chondrocyte adhesion, shape, proliferation, cytokinesis, and actin organization. In addition, the cartilage matrix shows a sparse, distorted collagen network. Similar, but milder abnormalities were found in mice lacking the collagen-binding integrin α10β1 or integrin-linked kinase in cartilage (11, 12).

Although these works have identified β1 integrins as essential regulators of growth plate development, the role of integrins in joint morphogenesis, adult joint function, and pathology is incompletely understood. In the embryonic mouse limb culture system, administration of β1 and α5 blocking antibodies or RGD peptides induced ectopic joint formation between proliferating and hypertrophic chondrocytes of the growth plate, suggesting that α5β1 integrin controls the decision

* This work was supported by grants from the Max Planck Society (to A. R. and A. A.) and the Swiss National Science Foundation (to E. B. H.).

[1] To whom correspondence should be addressed. Tel.: 49-89-8578-2466; Fax: 49-89-8578-2422; E-mail: aszodi@biochem.mpg.de.

[2] The abbreviations used are: AC, articular cartilage; ECM, extracellular matrix; PG, proteoglycan; GAG, glycosaminoglycan; OA, osteoarthritis; MMP, matrix metalloproteinase; ADAMTS, a disintegrin and metalloproteinase with thrombospondin-like repeat; FN, fibronectin; FN-f, fibronectin fragment; MAPK, mitogen activated protein kinase; ERK, extracellular signal-regulated kinase; JNK, c-Jun NH_2-terminal kinase; HE, hematoxylin and eosin; SO, safranin orange; PM, pericellular matrix; ITM, interterritorial matrix; PCNA, proliferating cell nuclear antigen; TUNEL, terminal deoxynucleotidyltransferase-mediated dUTP nick end labeling; IHC, immunohistochemistry; PFA, paraformaldehyde; PBS, phosphate-buffered saline; FAK, focal adhesion kinase; X-gal, 5-bromo-4-chloro-3-indolyl-β-D-galactopyranoside.

between cartilage differentiation and joint formation during development (13). In adult joints, increased immunostaining of β1 integrin was reported in osteoarthritic monkey cartilage compared with normal cartilage (14) and in human OA samples at minimally damaged locations compared with areas with more severe lesions (15). In another study, the neoexpression of α2, α4, and β2 integrins was observed in osteoarthritic human femoral head cartilage (16). *In vitro* experiments have suggested that signaling through the fibronectin (FN) receptor α5β1 integrin is pivotal to prevent cell death of normal and osteoarthritic human articular chondrocytes (17). FN fragments (FN-fs) present in synovial fluid and cartilage of OA patients have been implicated in cartilage breakdown (18–21). Human AC chondrocytes treated with the central, 110–120-kDa cell-binding FN-f but not with intact FN were shown to increase MMP-13 synthesis through the stimulation of α5β1 integrin and the subsequent activation of the proline-rich tyrosine kinase-2 and mitogen-activated protein kinases (MAPKs) ERK-1/2, JNK, and p38 (22, 23). Similarly, an adhesion-blocking antibody against α2β1 integrin induced the phosphorylation of MAPKs in human AC chondrocytes (22). Treatment of cultured rabbit synovial fibroblasts with central FN-fs or activating antibodies against α5β1 integrin elevated MMP-1 and MMP-3 expression (24). Although these experiments suggest that blocking integrin signaling through α2β1/α5β1 in response to degradation fragments may attenuate OA, mice lacking α1β1 integrin are prone to osteoarthritis (25). Knee joints of α1-null mice display precocious PG loss, cartilage erosion associated with increased MMP-2 and MMP-3 expression, and synovial hyperplasia.

To further explore the role of β1 integrins in joint biology, here we report the deletion of the floxed β1 integrin gene in embryonic limb bud mesenchymal cells using the *Prx1cre* transgene (26). $\beta1^{fl/fl}$-*Prx1cre*$^{+}$ mice were born alive with short limbs due to the lack of β1 integrin heterodimers on chondrocytes. We found that β1 integrin deficiency in knee joints leads to multiple abnormalities of the AC and the synovium, but it is not associated with accelerated AC destruction, perturbed AC metabolism, and MAPK signaling. Our data suggest that β1 integrins are required for the proper structural organization of the AC by anchoring chondrocytes to the ECM, but signaling through β1 integrins is less important for normal cartilage homeostasis.

EXPERIMENTAL PROCEDURES

Mice and Radiography—Conditional β1 integrin mutant mice ($\beta1^{fl/fl}$-*Prx1cre*$^{+}$) were generated by intercrossing homozygous floxed (fl) β1 integrin females (27) with males double heterozygous for the β1 integrin ($\beta1^{fl/+}$) and *Prx1cre* transgenic alleles (26). $\beta1^{fl/+}$-*Prx1cre*$^{+}$ and $\beta1^{fl/+}$-*Prx1cre*$^{-}$ mice were phenotypically indistinguishable; therefore, both genotypes were used as controls. For x-ray analysis, 16-month-old mice were euthanized, and radiographs were taken with a sealed x-ray cabinet (Faxitron model 43855A) at 35 kV, 2 mA, and 2 s of exposure time.

Histology, Histopathological Grading, and X-gal Staining—Control and $\beta1^{fl/fl}$-*Prx1cre*$^{+}$ mice were euthanized, and knee joints were harvested at various time points. For histology, samples were fixed in 4% paraformaldehyde (PFA) in phosphate-buffered saline (PBS, pH 7.4), decalcified in 10% EDTA-PBS, and processed for paraffin embedding. Approximately 300 consecutive, 6-μm-thick sagittal sections were collected from each specimen, and every 10th section was stained with hematoxylin-eosin (HE) for general histology or safranin O-Fast green (SO) to monitor PG depletion. Thus, about 30 serial sections representing the entire knee joint were evaluated from every mouse within each genotype and age group. Comparable sections for photography were chosen with the help of anatomical structures of the joint, such as the position of the menisci or the cruciate ligaments.

To determine cell density, digital images of HE-stained sections of the tibial plateau of each specimen were combined and analyzed by Adobe Photoshop CS2. The number of cells in the whole depth of the AC (from the surface to the osteochondral junction) was counted in at least four optical sections, and cellularity was expressed as a mean number of chondrocytes/0.01 mm^2. Total articular cartilage thickness and thicknesses of uncalcified and calcified cartilages were measured on three representative SO-stained sections at three different regions (lateral, middle, and medial) in at least five animals of each genotype at each age.

To assess pathological changes of the articular cartilage, we used a scoring system as follows: I, cartilage erosion (0–5; 0, smooth cartilage surface; 1, surface irregularities; 2, cleft to transition zone; 3, cleft to radial zone; 4, cleft to calcified zone; 5, exposure of subchondral bone; II, cellularity (0–3; 0, normal; 1, hypercellularity; 2, clustering; 3, hypocellularity); III, tidemark integrity (0–1; 0, normal; 1, loss of tidemark); IV, GAG content in the pericellular matrix (PM) (0–2; 0, normal SO staining intensity; 1, focally increased intensity; 2, increased intensity throughout the cartilage); V, GAG content in the interterritorial matrix (ITM) (0–3; 0, normal SO staining intensity; 1, reduced staining; 2, focal patchy loss of staining; 3, 50% of cartilage without staining; VI, osteophyte formation (0–2; 0, none; 1, formation of cartilage; 2, formation of bone). Total scale (0–16) and OA severity were as follows: 0–1, normal; 2–5, mild OA; 6–11, moderate OA; 12–16, severe OA.

Picrosirius red and X-gal stainings were performed as described elsewhere (28, 29). Picrosirius red-stained sections were analyzed by polarization microscopy for collagen deposition. The intensity of the collagen birefringence in polarized light is proportional with the amount of oriented collagen molecules.

Ultrastructural Analysis—Knee joints, including the subchondral bone, were isolated, and the tibial and femoral sides were separated under a stereomicroscope. Specimens were fixed in 2% glutaraldehyde in 0.1 M sodium cacodylate buffer (pH 7.4) for 3 days and processed for electron microscopy as previously described (30).

Analysis of the Actin Cytoskeleton—Tibiae were freshly dissected, and ~80-μm-thick sagittal sections were obtained using a vibratome (Microm). Sections were then fixed in 4% PFA/PBS for 2 h at room temperature, permeabilized with 0.1% Triton X-100, and stained with phalloidin Alexa488 (Molecular Probes catalog number A12379; dilution 1:200) at 4 °C overnight to visualize the actin cytoskeleton and subsequently with

4′,6-diamidino-2-phenylindole (Sigma catalog number D9542; 100 ng/ml) for 5 min to visualize the nucleus.

Chondrocyte Proliferation and Apoptosis—To assess chondrocyte proliferation, proliferating cell nuclear antigen (PCNA) immunostaining (see below) was performed on tissue sections. To determine the labeling index, the percentage of immunoreactive nuclei per 100 cells, the numbers of brown-colored nuclei were counted. To detect apoptotic cells, a TUNEL assay was used as described in Ref. 10.

Reverse Transcription-PCR—To examine the mRNA levels of matrix-degrading enzymes, tibiae were harvested from 4-month-old control and $\beta1^{fl/fl}$-*Col2a1cre*$^{+}$ mice. Vibratome sections (100 μm) were cut, and the articular cartilages were dissected using a sharp blade and a stereomicroscope. Cartilage pieces were pooled, and total RNA was isolated using the RNeasy lipid tissue minikit (Qiagen). The cDNA was synthesized using SuperScript III RNase H^{-} reverse transcriptase (Invitrogen). For semiquantitative reverse transcription-PCR, the following primers were used: $Mmp2_{forward}$ (5′-GACAAGTGGTCCGCGTAAAG) and $Mmp2_{reverse}$ (5′-CATCTGCATTGCCACCCATG); $Mmp3_{forward}$ (5′-CCTACTTCTTTGTAGAGGAC) and $Mmp3_{reverse}$ (5′-GTCAAATTCCAACTGCGAAG); $Mmp8_{forward}$ (5′-GTAAACTGTAGAGTCGATGC) and $Mmp8_{reverse}$ (5′-CATAGGGTGCGTGCAAGGAC); $Mmp9_{forward}$ (5′-CGAGTGGACGCGACCGTAGTTGG) and $Mmp9_{reverse}$ (5′-CAGGCTTAGAGCCACGACCATACAG); $Mmp13_{forward}$ (5′-GTGTGGAGTTATGATGATGT) and $Mmp13_{reverse}$ (5′-TGCGATTACTCCAGATACTG); $Gapdh_{forward}$ (5′-TCGTGGATCTGACGTGCCGCCTG) and $Gapdh_{reverse}$ (5′-ACCCTGTTGCTGTAGCCGTAT). PCRs were performed three times using two independent cDNA preparations as templates.

Antibodies and Immunohistochemistry—Primary antibodies and dilutions used were as follows: rabbit anti-ADAMTS4 (Chemicon catalog number AB19165; 1:500); rabbit anti-ADAMTS5 (Abcam catalog number ab13976; 1:500); rabbit anti-aggrecan (Chemicon catalog number AB1031; 1:1000); rat anti-β1 integrin (Chemicon catalog number MAB1997; 1:400); rabbit anti-C1,2C (IBEX catalog number 50-1035; 1:200); rat-anti-collagen II (a gift from Rikard Holmdahl (Karolinska Institute, Stockholm); 1:400); rabbit anti-collagen VI (a gift from the late Rupert Timpl (MPI for Biochemistry); 1:1000); rabbit anti-collagen X (a gift from Björn Olsen (Harvard Medical School, Boston, MA); 1:500); rabbit anti-G1-TEGE (Acris catalog number SP5418P; 1:500); rabbit anti-G1-PEN (a gift from Amanda Fosang (University of Melbourne); 1:4000); mouse-anti-MMP-1 (Calbiochem catalog number IM35L; 1:50); rabbit anti-MMP-2 (Chemicon catalog number AB19167; 1:400); mouse anti-MMP-3 (Oncogene Research Products catalog number IM70; 1:50); rabbit anti-MMP-9 (Chemicon catalog number AB19016; 1:400); goat anti-MMP-13 (Chemicon catalog number AB8120; 1:400); mouse anti-PCNA (Dako catalog number M879); rabbit anti-phospho-ERK1/ERK2 (catalog number 4376, 1:100), rabbit anti-phospho-JNK (catalog number 9251, 1:50), and rabbit anti-phospho-p38 (catalog number 4631; 1:50) (all obtained from Cell Signaling); and rabbit anti-phospho-FAK (pY397; Invitrogen catalog number 44624G; 1:100).

For immunohistochemistry, knee joints were fixed in 4% PFA/PBS overnight, decalcified in 10% EDTA-PBS, and processed either for paraffin embedding or cryoembedding. Sections (6 μm) were deparaffinized and/or rehydrated and digested with bovine testicular hyaluronidase (2 mg/ml in PBS, pH 5.0) at 37 °C for 30 min to enhance antibody penetration. In the case of phospho-ERK, -JNK, and -p38 and PCNA, antigen retrieval was performed in 6 M guanidine hydrochloride, 50 mM Tris-HCl (pH 7.6) for 15 min at room temperature, followed by permeabilization in a solution containing 0.5% Triton X-100 in PBS for 15 min. The sections were than submerged in 0.3% hydrogen peroxide/methanol solution for 30 min to quench endogenous peroxidase activity and blocked with 1.5% normal serum, 1% bovine serum albumin for 60 min at room temperature. Afterward, the slides were incubated with primary antibodies at 4 °C overnight in the blocking solution and immunostained by the avidin-biotin complex method using the appropriate Vectastain ABC Elite kit (Vector Laboratories catalog number PK-6101 for rabbit IgG, PK-6104 for rat IgG, and PK-6105 for goat IgG) or the Vector M.O.M. peroxidase immunodetection kit (Vector Laboratories catalog number PK-2200 for mouse IgG) and 3,3′-diaminobenzidine (Sigma) as chromogenic substrate. Sections were counterstained with hematoxylin and mounted with Aquatex (Merck). Images, representative of those obtained from the knee joints of at least 4 mice/group at each age, were taken by a Zeiss Axioskop light microscope attached to a Leica DC500 digital color camera. The specificity of the reactions was controlled by omitting the primary antibody (negative control) or by incubating sections with non-immune IgG (IgG control) in the same concentration as the less diluted primary antibody (Vector Laboratories; rabbit IgG I-1000, goat IgG I-5000, rat IgG I-4000, and mouse IgG I-2000).

Enzyme-linked Immunosorbent Assays—Commercial enzyme-linked immunosorbent assay kits were used to detect the levels of collagen II degradation products either in urine samples (CTX-II, which measures C-telopeptides fragments; Nordic Bioscience catalog number 2CAL4000) or in serum samples (C2C, which measures the carboxyl-terminal three-fourths fragment collagen II cleavage neoepitope; IBEX catalog number 60-1001-001). The CPII enzyme-linked immunosorbent assay kit (IBEX catalog number 60-1003-001) was used to measure the serum level of collagen II C-propeptide, which correlates with collagen II biosynthesis. Urine samples obtained by gentle abdominal pressure from each mouse were collected into plastic tubes and frozen at −20 °C until use. Blood samples were than collected individually from the vena cava inferior of each mouse, allowed to coagulate at room temperature for 1 h, and centrifuged at 600 × *g* for 10 min. Sera were aliquoted, rapidly frozen, and stored at −70 °C until the assay. Analyses were performed by keeping the same gender ratio of control and mutant mice at each age.

Cartilage Explant Culture—Femoral heads were harvested from 4-week-old control and mutant mice and cultured in 300 μl of serum-free Dulbecco's modified Eagle's medium supplemented with streptomycin-penicillin in a 48-well plate for 4 days. Treated cartilages received a 1 μM fibronectin fragment (40.1-kDa FNIII7-10RGD) from the beginning of the culture. At the end of the culture period, the femoral heads were fixed in 4% PFA/PBS and cryoembedded. Sections from treated and

untreated as well as from day 0 samples were immunostained for phospho-ERK1/ERK2 and MMP-13.

Statistical Analysis—Nonparametric Mann-Whitney *U* test was used to compare the median of total histopathology and cartilage erosion scores. All other data were expressed as the mean ± S.D. or the means ± S.E. Significance was assessed using unpaired Student's *t* test.

RESULTS

Generation of the $\beta1^{fl/fl}$-Prx1cre^{+} Mice—To assess the function of β1 integrins in joint biology, we deleted the floxed β1 integrin gene in embryonic limb bud mesenchyme by using the *Prx1cre* transgenic line (26). Since the ablation of the $\beta1^{fl}$ allele activates a promoterless *LacZ* gene (10), we performed X-gal staining to demonstrate β-galactosidase activity and monitor the deletion of the gene. Forelimb sections of $\beta1^{fl/fl}$- *Prx1cre*$^{+}$ mice at embryonic day 18.5 showed β-galactosidase activity in tissues of mesenchymal origin, including cartilage, periosteum/perichondrium, ligaments, tendons, synovium, and vessels (Fig. 1, *A–D*). Although β-galactosidase-negative chondrocytes were occasionally observed in the growth plate, the developing AC contained only β-galactosidase-positive chondrocytes, indicating very high deletion efficiency of β1 integrin in this region (Fig. 1*B*).

$\beta1^{fl/fl}$-*Prx1cre*$^{+}$ mice recapitulate the embryonic skeletal phenotype of $\beta1^{fl/fl}$-*Col2a1cre*$^{+}$ mice (not shown) and survive after birth. Immunostaining of control knee joints at 1 month showed abundant expression of β1 integrin on AC chondrocytes, whereas little if any expression was detected in $\beta1^{fl/fl}$-*Prx1cre*$^{+}$ AC (Fig. 1*E*). Similarly, β1 integrin was largely absent in the synovium (Fig. 1*F*), meniscus, patella, and joint ligaments (not shown). Adult mutant mice exhibited shortened long bones and abnormal gait, which were associated with reduced flexibility of the knee joints from 7 months. X-ray analysis of the hind limb at 16 months (Fig. 1*G*) demonstrated misaligned bones, irregular joint surfaces, joint space narrowing, and the appearance of radio-dense plaques in the vasculature of $\beta1^{fl/fl}$-*Prx1cre*$^{+}$ mice. The mutant mice were able to walk at all stages; however, their mobility was apparently reduced from 8 months of age compared with control littermates. The frequency of vascular calcification increases with age and is associated with high mortality rate between 8 and 12 months of age.

Histopathological Changes of the Articular Cartilage—At birth, the forming AC in control and mutant tibiae was unstratified, with rounded chondrocytes exhibiting a random, isotropic distribution pattern (Fig. 2*A*). At 2 weeks of age, control mice developed well formed secondary ossification centers in both the femur and the tibia, whereas only some hypertrophy but no ossification of the epiphyses was visible in mutants (not shown). At 1 month, ossification appeared in the mutant femoral epiphysis, whereas the secondary ossification center of the tibia was narrowed and entirely composed of chondrocytes (Fig. 2*B*). Control AC displayed structural anisotropy characterized by the appearance of flattened chondrocytes at the superficial layer and formation of columns in deeper regions. In contrast, the mutant AC was still isotropic, lacking flat cells and column-like structures and showed a broad, acellular surface area facing the joint cavity (Fig. 2*C*). After 1 month of age, ossification was also evident in the mutant tibia, and the AC exhibited several abnormalities, including thickening (Fig. 2*I*), disorganized cell arrangement with frequent clustering, flattening of the tibial plateau, and formation of less subchondral bone (Fig. 2*D*). In 1- and 4-month-old control and mutant mice, the AC surface was largely intact with slightly increased roughening in mutants (Fig. 2*C*) (data not shown). At 7 months, we found

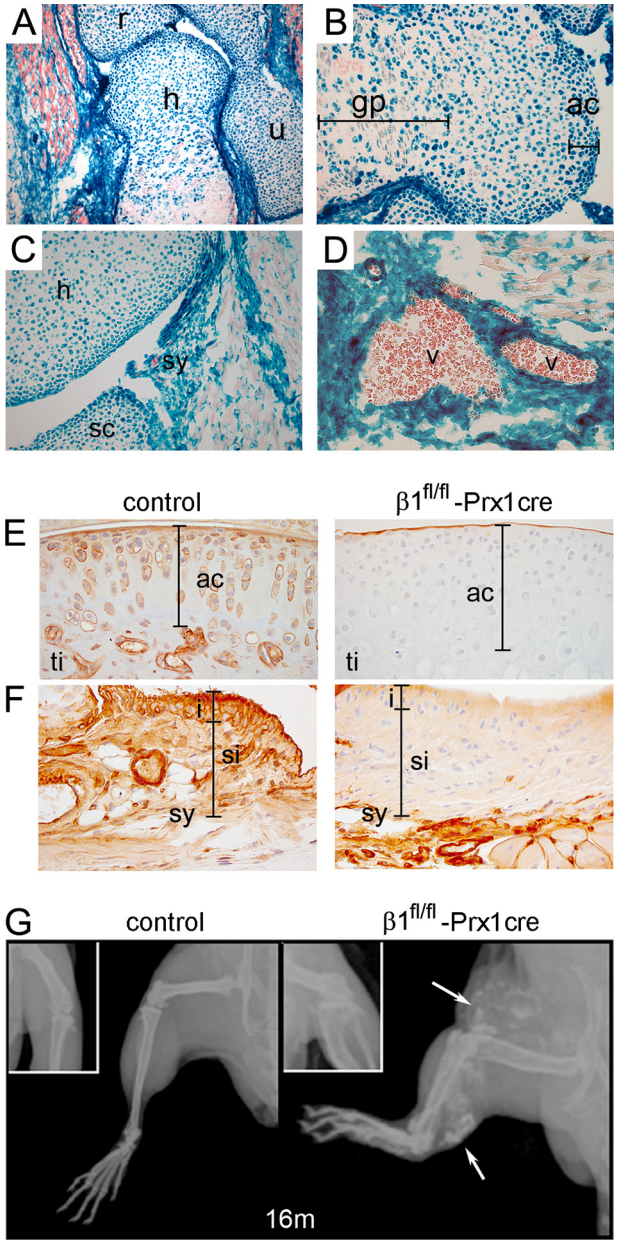

FIGURE 1. **Deletion of the β1 integrin gene in mice using the *Prx1-cre* transgenic line.** *A*, X-gal staining of a forelimb section from $\beta1^{fl/fl}$-*Prx1cre*$^{+}$ embryonic day 18.5 embryo shows Cre recombinase activity in cartilaginous and bony tissues of the elbow and in muscle fibroblasts (*h*, humerus; *r*, radius; *u*, ulna). *B*, distal epiphysis of the humerus exhibits Cre activity in all chondrocytes (*blue*) of the presumptive articular cartilage (*ac*), whereas in the growth plate (*gp*), some chondrocytes (*red*) are negative. *C* and *D*, X-gal staining demonstrates Cre activity in the forming synovium (*sy*) (*C*) and in the vessels (*v*) (*D*). *E* and *F*, β1 integrin immunostaining at 1 month of age demonstrates the absence of β1 integrin on articular cartilage chondrocytes of mutant tibia (*ti*) (*E*) and on synoviocytes of the synovium (sy) (*F*). The *bars* on *F* indicate the intimal (*i*) and subintimal (*si*) layers of the synovium. *G*, x-ray of the hind limb at 16 months indicates short bones, joint space narrowing, and blood vessel calcification (*arrows*) in mutants.

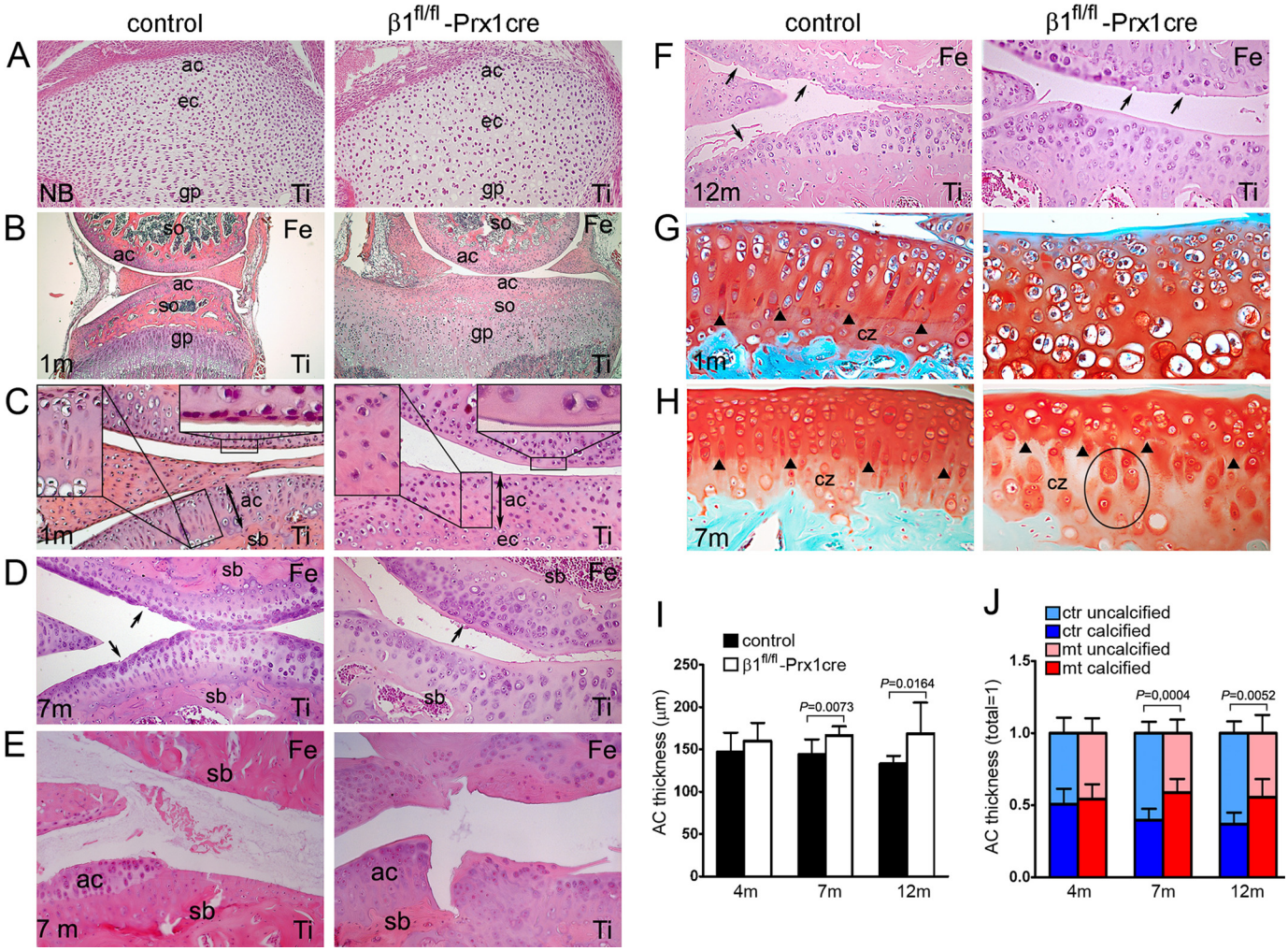

FIGURE 2. **Comparison of the articular cartilage from the knee joints of control and *β1*$^{fl/fl}$*-Prx1cre*$^{+}$ mice.** *A–D*, photomicrographs of hematoxylin-eosin-stained sections (*Ti*, tibia). *A*, in newborn (*NB*), both control and mutant articular cartilage (*ac*) chondrocytes are rounded and exhibit an isotropic distribution pattern (*ec*, epiphyseal cartilage; *gp*, growth plate). *B*, at 1 month (*1m*), *β1*$^{fl/fl}$*-Prx1cre*$^{+}$ joints show a delay in the formation of the secondary ossification center (*so*) and display flat tibial surface. *C*, closer view from *B* indicates fewer chondrocytes, a broad, cell-free superficial layer (*upper right inset*), and the lack of column-like structures (*upper left inset*) in mutant AC. Subchondral bone (*sb*) does not form in the mutant tibia at this age. *D*, micrographs demonstrate surface irregularities (*arrows*) of control and mutant articular cartilage of female mice at 7 months of age. Chondrocyte columns are missing, and less subchondral bone forms in mutants. *E*, 7-month-old male mice display AC defects exposing the subchondral bone. *F*, at 12 months, erosion typically extends into the radial zone of control AC and into the transition zone of mutant AC. *G* and *H*, photomicrographs of safranin orange-Fast green-stained sections through the medial tibial plateau. At 1 month (*G*), chondrocyte clustering, structural disorganization, and the lack of tidemark are characteristic for the mutant articular cartilage. In control, the tidemark (*arrowheads*) separates the calcified zone (*cz*) from the upper uncalcified region. At 7 months (*H*), the mutant articular cartilage is thicker with expanded calcified and reduced uncalcified zones. Note the enlarged pericellular matrix staining around mutant chondrocytes (*ellipses*) in the calcified zone. *I*, quantification of the AC thickness. *J*, quantification of the ratio of uncalcified and calcified zones. The total AC thicknesses were set as 1. *Bars* in *I* and *J* represent the mean ± S.D.; $n = 8/8$ at 4 months, $n = 10/10$ at 7 months, and $n = 9/8$ at 12 months (where n = number of control mice/number of mutant mice). In each control and mutant animal, three comparable regions of the tibial AC were analyzed. Statistical significance was determined by an unpaired *t* test.

obvious signs of cartilage erosion in both experimental groups, ranging from surface irregularities to the exposure of the subchondral bone (Figs. 2 (*D* and *E*) and *3B*). We have noticed that female mice displayed milder destruction than male mice (Fig. 3*B*). At 12 months, clefts typically extended into the radial zone in controls, whereas mutants surprisingly exhibited less severe erosion with clefts usually not extending below the transition zone (Figs. 2*F* and 3*B*). In general, SO staining indicated comparable levels of negatively charged PGs in control and mutant AC (Fig. 2, *G* and *H*). At 1 month, the tidemark separating the uncalcified and calcified AC was only detectable in controls (Fig. 2*G*). At later stages, the tidemark appeared in the mutants; however, it was irregular and often discontinuous (Fig. 2*H*). Typically, extended PM staining was observed in the calcified zone of mutants. Furthermore, the length of the uncalcified zones with strong SO staining in the ITM is decreased, whereas the length of the calcified zone with less intense staining in the ITM is increased in mutants (Fig. 2, *G*, *H*, and *J*). The abnormalities of the mutant AC were not restricted to the knee region. Similar features (*e.g.* structural disorganization, AC thickening, and chondrocyte rounding) were also prominent in the hip joint and in the ankle (not shown).

Quantification of the histopathological changes of the knee joint revealed that the total score (the sum of subscores; see "Experimental Procedures") is increased in each age group (4, 7, and 12 months) of mutants compared with controls (Fig. 3*A*). Separate evaluation of cartilage erosion, however, did not reveal significant differences in AC destruction between control and

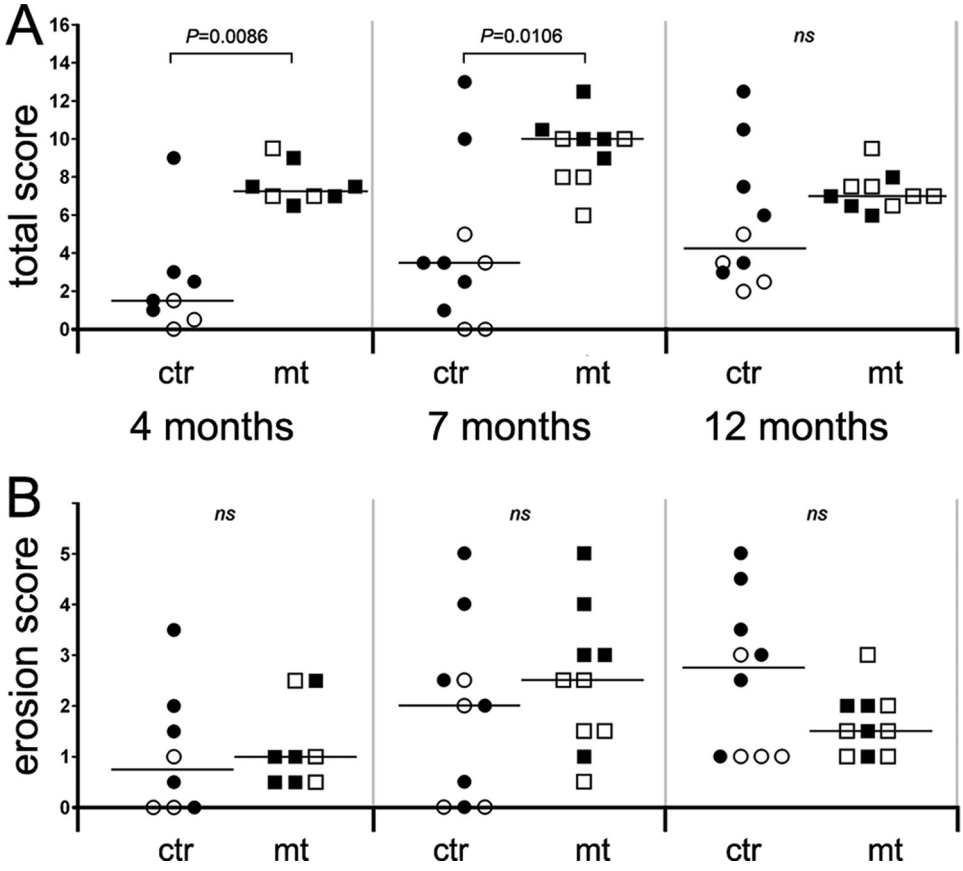

FIGURE 3. **Quantification of the histopathological changes of the knee.** *A*, total score indicates increased severity of joint histopathology in mutants at 4 and 7 months of age. By 12 months, the differences between controls (*ctr*) and mutants (*mt*) are not significant (*ns*). *Open symbols*, female mice; *filled symbols*, male mice. *B*, quantification of cartilage erosion reveals no significant difference in articular cartilage destruction between controls and mutants. *Horizontal lines* in *A* and *B* represent the median values; $n = 8/8$ at 4 months, $n = 10/10$ at 7 months, and $n = 10/10$ at 12 months (where n = number of control mice/number of mutant mice). For each animal, 30 HE- and SO-stained sections representing the entire knee region were analyzed. Statistical differences between genotype groups were evaluated using the Mann-Whitney *U* test.

mutant mice (Fig. 3*B*). Although the median score was slightly higher in mutants at 4 and 7 months, it moderately decreased at 12 months compared with controls.

Ultrastructural and Cytoskeletal Abnormalities of the Mutant Articular Cartilage—Electron microscopy at 4 months revealed abnormalities throughout the mutant AC (Fig. 4*A*). Compared with controls, mutant mice displayed an enlarged superficial zone with extra layers of disorganized collagen fibrils and rounded chondrocytes. In all AC zones, the PM compartment was expanded, most prominently in the lower radial and the calcified zones; the chondrocytes were frequently binucleated and extended long microvilli into the matrix. In the ITM compartment, the fibrillar network was less organized, with a high variation of fibril density (not shown), whereas in the PM, thick collagen bundles occasionally appeared near the chondrocyte surface (Fig. 4*A*).

To test the impact of β1 integrin deficiency on the actin cytoskeleton of AC chondrocytes, we analyzed phalloidin-stained tissue sections by confocal microscopy. At 4 months, the actin network was only mildly affected in mutants (not shown); however, by 11 months, marked abnormalities of the cytoskeleton were observed in chondrocytes located at the weight-bearing regions of the tibial plateau (Fig. 4*B*). Whereas control chondrocytes in the uncalcified zones exhibited a strong and even cortical actin staining, mutant chondrocytes showed a faint and punctate actin distribution, indicating a disrupted actin cytoskeleton in the absence of β1 integrins.

Chondrocyte Proliferation and Survival—Quantification of AC cellularity in the tibial plateau revealed that $\beta1^{fl/fl}$-*Prx1cre*$^{+}$ mice have reduced chondrocyte density (Fig. 5*A*). 1-month-old samples showed only a moderate reduction, whereas at later stages the mutants showed significantly fewer chondrocytes per unit area compared with controls. To study the underlying mechanism of hypocellularity, chondrocyte proliferation and death were investigated. Using PCNA immunostaining, we observed a normal proliferation rate at day 4; however, at 2 weeks, the fraction of PCNA-positive cells was reduced by about 25% in mutants (Fig. 5*B*). At 1 and 4 months of age, the PCNA index was very low and comparable in mutant and control samples. A closer view at 2 weeks revealed that in controls, most PCNA-positive cells were located throughout the AC, including the most superficial layer, whereas in mutants, PCNA-labeled chondrocytes were more prominent in deeper zones and were frequently binucleated (Fig. 5*C*). Because abnormal cytokinesis could also contribute to the reduced cell density, the binucleation rate of tibial plateau chondrocytes was quantified (Fig. 5*D*). The percentage of binucleated chondrocytes increased with age from 0.89% (1 month) to 1.62% (4 months) and to 2.19% (10 months) in control, whereas in the mutant, the binucleation rate was 5% at 1 month, and it increased to 7.66 and 10.57% by the age of 4 and 10 months, respectively. Assessing cell death by a TUNEL assay, we observed no difference in the apoptotic rates at 4 and 12 months; however, the percentage of TUNEL-positive chondrocytes was significantly higher at 7 months in the mutants (Fig. 5*E*).

The Expression of Collagen X and Collagen VI Is Altered in the Mutant AC—IHC showed that the expression and deposition of most ECM molecules, including aggrecan and collagen type II, were apparently normal in the mutant tibial plateau cartilage (not shown). In contrast, collagen X, which is produced by hypertrophic chondrocytes and present in the calcified zone of the AC, displayed an abnormal staining pattern (Fig. 6*A*). In controls, collagen X was detectable below the tidemark at a distance of 6–7 cell layers from the surface, whereas in $\beta1^{fl/fl}$-*Prx1cre*$^{+}$ AC, collagen X appeared at a distance of 2–3 cell

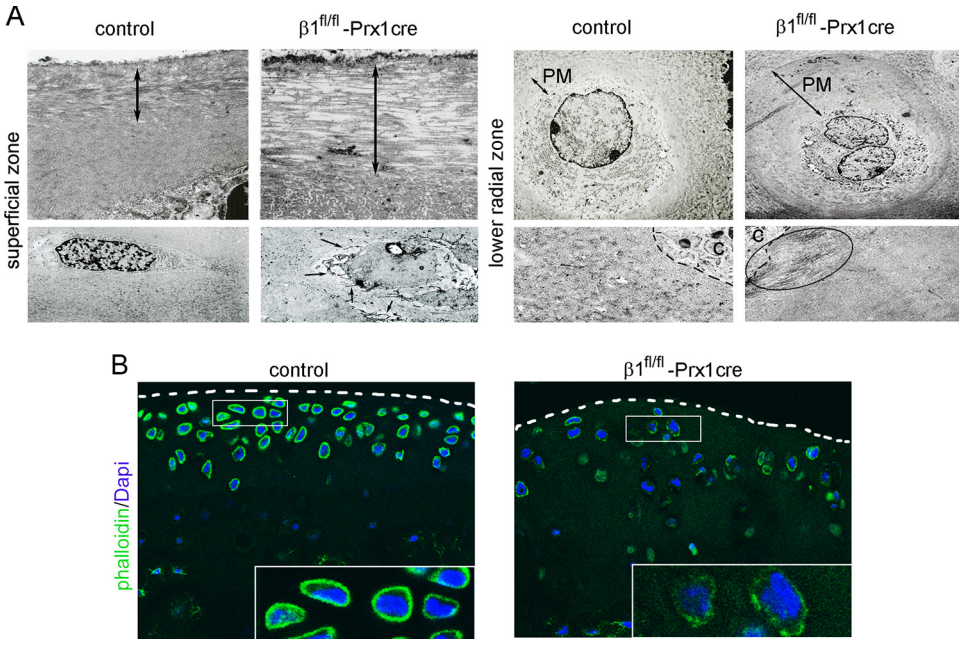

FIGURE 4. **Electron and confocal microscopy of articular cartilage from control and $\beta1^{fl/fl}$-$Prx1cre^{+}$ mice.** *A*, representative electron micrographs of the cartilage surface (superficial zone) reveal additional disorganized layers of collagen fibrils (*double arrow*) in the mutant sample. The superficial chondrocytes are more rounded and extend long microvilli into the matrix (*arrows*). In the lower radial zone, the mutant cartilage displays frequent binucleation, an enlarged PM compartment, and large collagen bundles near the chondrocyte surface (*ellipse*). *B*, confocal micrographs of 80-μm-thick vibratome sections stained for phalloidin (to visualize actin; *green*) and 4′,6-diamidino-2-phenylindole (*Dapi*) (to visualize nuclei; *blue*) from tibial plateau of 11-month-old mice demonstrate a reduced and irregular cortical actin network in $\beta1^{fl/fl}$-$Prx1cre^{+}$ chondrocytes. The *dashed lines* demarcate the surface of the articular cartilage. The *insets* show magnified images of control and mutant chondrocytes. The pictures are representative of experiments performed with tissues obtained from three different control and mutant animals.

layers, consistent with the reduced depth of the uncalcified cartilage. Occasionally, mutant cells in the uncalcified zone displayed strong collagen X deposition, suggesting premature differentiation of $\beta1^{fl/fl}$-$Prx1cre^{+}$ chondrocytes. Furthermore, collagen VI was detectable in the PM of all control cells in the uncalcified zones, but it was apparently missing at certain locations around mutant chondrocytes (Fig. 6*B*).

The Lack of β1 Integrin on Chondrocytes Does Not Lead to Detectable Changes in Articular Cartilage Metabolism—To assess the expression of matrix-degrading enzymes, first the mRNA levels of *Mmp2*, *Mmp8*, *Mmp9*, and *Mmp13* were examined by semiquantitative reverse transcription-PCR at 4 months of age. In three independent experiments, we found comparable levels of MMP mRNAs in control and $\beta1^{fl/fl}$-$Prx1cre^{+}$ mice (Fig. 7*A*). Next, we performed immunostaining for MMP-1, MMP-2, MMP-3, MMP-9, MMP-13, ADAMTS-4, and ADAMTS-5. In general, the expression of MMPs was low or undetectable in the AC, and no significant differences were observed between mutant and control samples at 4, 7, and 12 months of age (Fig. 7*B*) (data not shown). ADAMTS-5 and ADAMTS-4 were evident around chondrocytes in the nonmineralized AC, and their expression was indistinguishable between control and $\beta1^{fl/fl}$-$Prx1cre^{+}$ mice (Fig. 7*B*) (data not shown). To further examine matrix catabolism, collagen and aggrecan degradation products were investigated on tissue sections by IHC (Fig. 7*C*). The aggrecan neoepitope G1-IPEN^{341} (generated by MMPs) was predominantly detectable in the calcified zone, whereas the G1-TEGE^{373} (generated by aggrecanases) was abundant in the pericellular matrix of chondrocytes in the uncalcified zones. We noticed no apparent changes in the amount of degraded aggrecan in $\beta1^{fl/fl}$-$Prx1cre^{+}$ mice compared with controls at 7 and 12 months. Similarly, there was no obvious difference in type II collagen degradation *in situ* judged by the C1,2C polyclonal antibody, which recognizes the Col2–3/4C$_{short}$ neoepitope upon cleavage by collagenases, such as MMP13 (Fig. 7*C*). Finally, serum or urine samples were investigated by enzyme-linked immunosorbent assays to detect type II collagen degradation (C2C and CTX-II) or synthesis (CPII) products. Again, no statistically significant differences were found between mutant and control samples (Fig. 7, *D–F*).

β1 Integrin Null Chondrocytes Display Normal Activation of MAPKs—Signaling pathways via MAPKs are activated by extracellular stimuli and may play an important role in joint destruction by regulating the expression of proinflammatory cytokines and MMPs (31). To check the activity of "classical" MAPKs in β1-deficient AC chondrocytes, we performed IHC using antibodies that specifically recognize the phosphorylated forms of ERK-1/2, p38, and JNK. At 1 month of age, numerous femoral head AC chondrocytes stained positive, and we observed no obvious differences in activation of MAPKs between controls and mutants (Fig. 8*A*). Next, femoral head articular cartilage was removed from control and mutant mice, cultured in serum-free medium with or without the central, cell binding fragment of fibronectin (FNIII7-10). After 4 days in culture, the explants were investigated for ERK phosphorylation and MMP-13 expression by IHC (Fig. 8*B*). In untreated samples, no ERK activation and MMP-13 deposition were observed in the articular cartilage. In contrast, both control and mutant articular cartilage that received FN-f exhibited comparable ERK phosphorylation and MMP-13 expression. These data indicate that FNIII7-10 fragments could stimulate MMP-13 expression via MAPK activation in the absence of the major FN-binding integrin α5β1. Finally, we analyzed the activation of the focal adhesion kinase (FAK), a central player of integrin signaling pathways, by using an antibody that recognizes the autophosphorylated Tyr^{397} residue. In agreement with previous results on growth plate chondrocytes (10), mutant AC chondrocytes at 2 weeks of age showed moderately decreased immunostaining compared with controls (not shown).

Histopathological Changes of the Synovial Tissue—Midsagittal sections through the developing knee joint at embryonic day 16 showed poorly differentiated synovium, collateral, and cru-

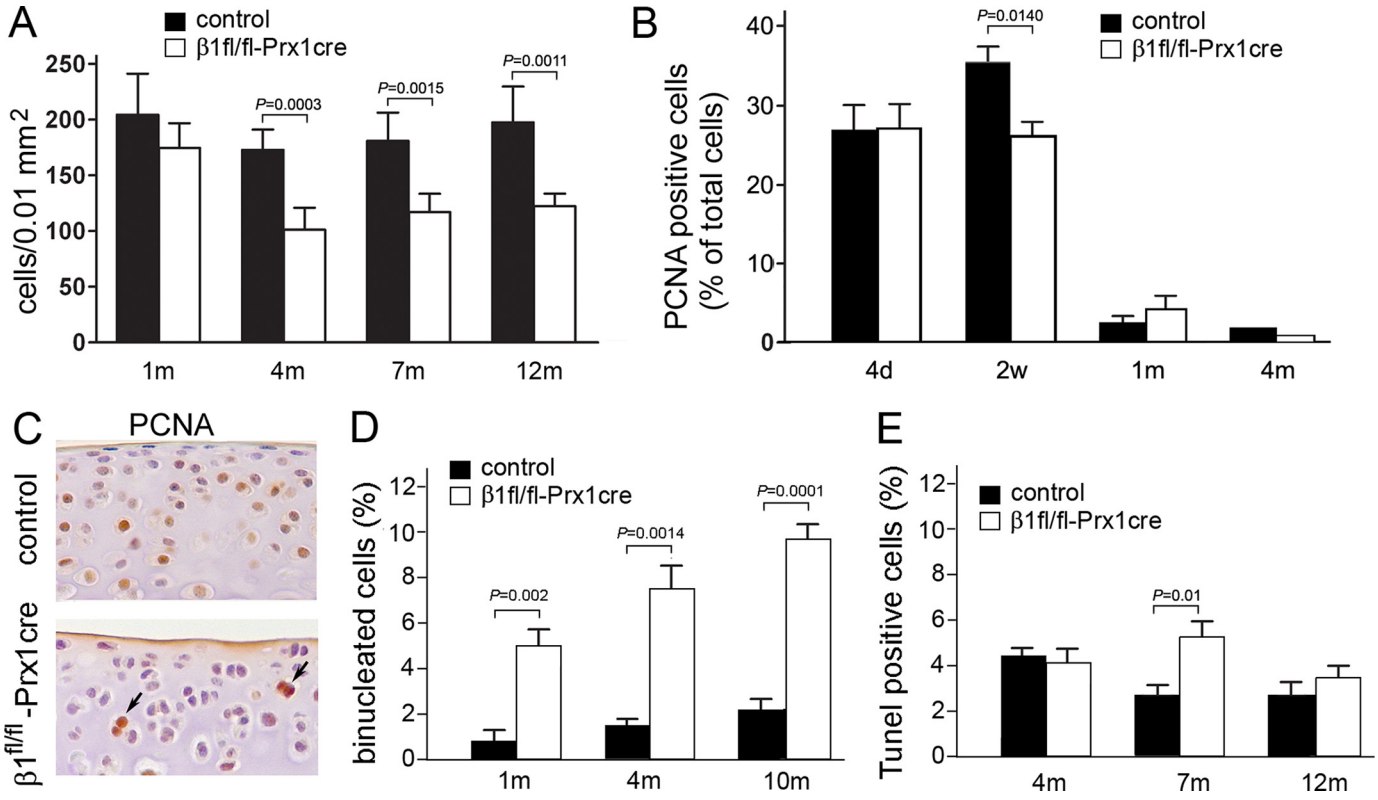

FIGURE 5. **Chondrocyte cellularity, proliferation, and survival in control and $\beta1^{fl/fl}$-*Prx1cre*$^{+}$ articular cartilage.** *A*, quantification of cell density at the tibial plateau demonstrates fewer chondrocytes per unit area in mutant than in control. *Bars*, mean ± S.D., unpaired *t* test, $n = 5$ at each age and genotype. *B*, percentage of PCNA-positive cells (mean ± S.D., unpaired *t* test). $n = 3$ at each age and genotype; $n_{control} = 707/2852$ (24.78%) and $n_{mutant} = 518/1925$ (26.90%) at 4 days, $n_{control} = 862/2497$ (34.52%) and $n_{mutant} = 779/2980$ (26.14%) at 2 weeks, $n_{control} = 16/742$ (2.15%) and $n_{mutant} = 48/1018$ (4.71%) at 1 month, and $n_{control} = 24/1194$ (2.01%) and $n_{mutant} = 8/998$ (0.80%) at 4 months (where n = number of PCNA positive cells/number of total cells). Note the moderately reduced proliferation rate in mutant at 2 weeks of age. *C*, PCNA immunostaining reveals the depletion of proliferative chondrocytes close to the articular surface compared with controls. The *arrows* indicate binucleated, PCNA-positive mutant chondrocytes in deeper regions of the articular cartilage. *D*, diagram showing the percentage of binucleated chondrocytes in control and mutant articular cartilage (mean ± S.D., unpaired *t* test; $n = 5$ at each age and genotype). *E*, percentage of apoptotic chondrocytes throughout the uncalcified articular cartilage (mean ± S.D., unpaired *t* test). $n = 3$ at each age and genotype; $n_{control} = 74/1688$ (4.38%) and $n_{mutant} = 56/1406$ (3.98%) at 4 months, $n_{control} = 101/3876$ (2.60%) and $n_{mutant} = 125/2285$ (5.47%) at 7 months, $n_{control} = 77/2818$ (2.73%) and $n_{mutant} = 55/1558$ (3.53%) at 12 months (where n = number of TUNEL-positive cells/number of total cells).

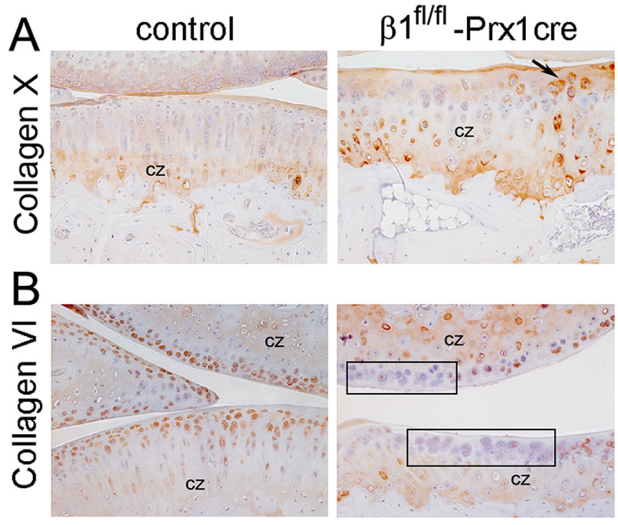

FIGURE 6. **Abnormal deposition of collagens X and VI in the mutant articular cartilage.** Immunohistochemical analysis of paraffin-embedded tissue sections. *A*, at 7 months, collagen X, a marker of the calcified zone (*cz*), appears closer to the cell surface in mutant compared with control. The *arrow* indicates mutant cells in the uncalcified zone depositing collagen X into the matrix. *B*, collagen VI is abundant in the pericellular matrix of control chondrocytes in the uncalcified zone. However, areas (*boxes*) with mutant chondrocytes in the uncalcified zone are devoid of immunoreactivity. Results are representative of those seen in five mice of each genotype.

ciate ligaments in $\beta1^{fl/fl}$-*Prx1cre*$^{+}$ mice compared with controls (Fig. 9*A*). In newborns, the control synovium was compact, and the joint ligaments were well developed, whereas in mutants, the synovial tissue had a loose appearance, the cruciate ligament was disorganized, and the collateral ligament was thinned (not shown). At 2 weeks, the control synovium was composed of a narrow lining layer and a large adipose compartment. The mutant synovium was hyperplastic (Fig. 9*B*) and showed fibrosis with extensive collagen deposits, revealed by strong birefringence under polarization microscopy (Fig. 9*C*). At 1 month, SO-stained sections through the nonarticular area of the control joints showed non-cartilaginous surfaces of the tibia and the femur interconnected by the cruciate ligaments, whereas the intercondylar surface of the mutant tibia was still cartilaginous (Fig. 9*D*). In mutant, the fibrotic synovial tissue invaded the joint space and began to undergo chondrogenic differentiation revealed by PG deposits, and by 7 months of age, the joint cavity was frequently filled with chondrophytes (Fig. 9, *D* and *E*). IHC at 2 weeks demonstrated increased numbers of PCNA-positive cells in the mutant synovium (Fig. 9*F*). In contrast to cartilage, increased phosphorylation of FAK was observed in the $\beta1^{fl/fl}$-*Prx1cre*$^{+}$ synovial tissue (Fig. 9*G*).

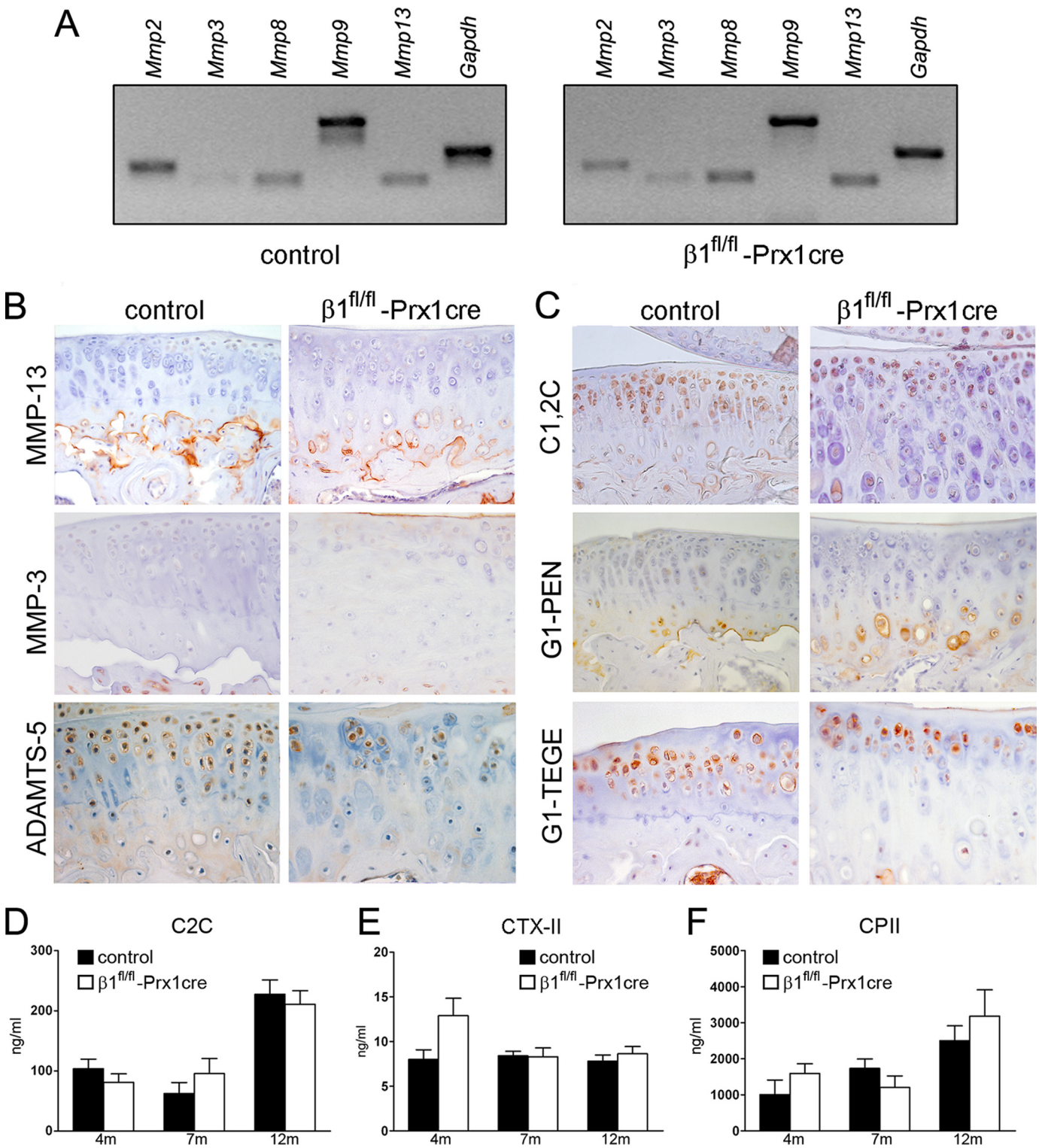

FIGURE 7. **Characterization of articular cartilage metabolism.** *A*, representative reverse transcription-PCR analysis at 4 months of age indicates that the levels of MMP mRNAs are comparable in control and mutant articular cartilage samples. *B*, immunohistochemistry on paraffin sections at 7 months reveals no changes in the deposition of MMP-13, MMP-3, and ADAMTS-5 in mutants compared with controls. *C*, immunohistochemistry on frozen sections at 7 months demonstrates that the degradation neoepitopes for collagen II (C1,2C) and aggrecan (G1-IPEN^{341} and G1-TEGE^{373}) are exposed similarly in mutant and control. The immunohistochemical results (*B* and *C*) are representative of those seen in five mice of each genotype. *D–F*, at 7 months, comparable levels of collagen degradation (C2C and CTX-II) and synthesis (CPII) products were found in serum (C2C, CPII) or urine (CTX-II) samples of control and *β1$^{fl/fl}$-Prx1cre^{+}* mice. Values are expressed as the mean ± S.E. of experiments carried out twice in duplicates (N_{C2C} = 5/7 at 4 months, N_{C2C} = 10/10 at 7 months, and N_{C2C} = 5/7 at 12 months; $N_{CTX\text{-}II}$ = 4/6 at 4 months, $N_{CTX\text{-}II}$ = 10/9 at 7 months, and $N_{CTX\text{-}II}$ = 6/6 at 12 months; N_{CPII} = 4/6 at 4 months, N_{CPII} = 8/6 at 7 months, and N_{CPII} = 7/8 at 12 months).

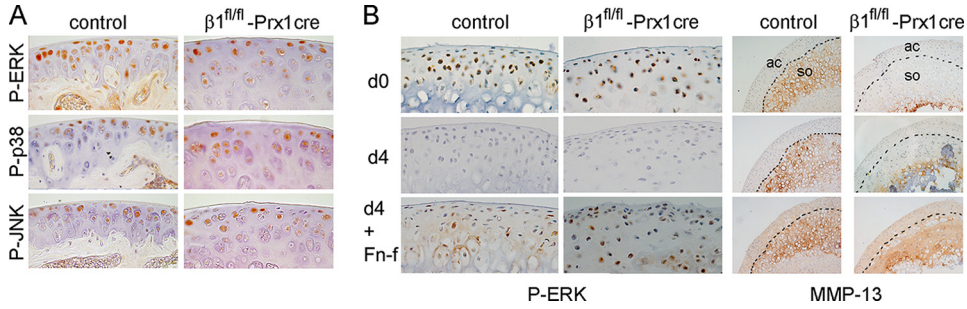

FIGURE 8. **Normal activation of MAPKs in the mutant articular cartilage.** *A*, immunostaining of paraffin sections for phospho-ERK1/2 (*P-ERK*), phospho-p38 (*P-p38*), and phospho-JNK (*P-JNK*) shows no detectable difference in the activation of MAPKs in control and mutant femoral head chondrocytes at 1 month of age. Results are representative of those seen in five mice of each genotype. *B*, FN-f stimulation of ERK activation and MMP-13 expression in femoral head explant culture. Shown is representative immunostaining performed on frozen sections of four experiments. At day 0 (*d0*), ERK is phosphorylated in many control and mutant chondrocytes. MMP-13 staining is visible only in the center of secondary ossification (*so*) but not in the articular cartilage (*ac*) of control samples. Due to the delay of terminal hypertrophic chondrocyte differentiation, mutant explants show only restricted MMP-13 deposition in the area of secondary ossification. At day 4 (*d4*), both control and $\beta1^{fl/fl}$-*Prx1cre*$^{+}$ samples treated with FN-f show ERK reactivation and MMP-13 expression in the articular cartilage.

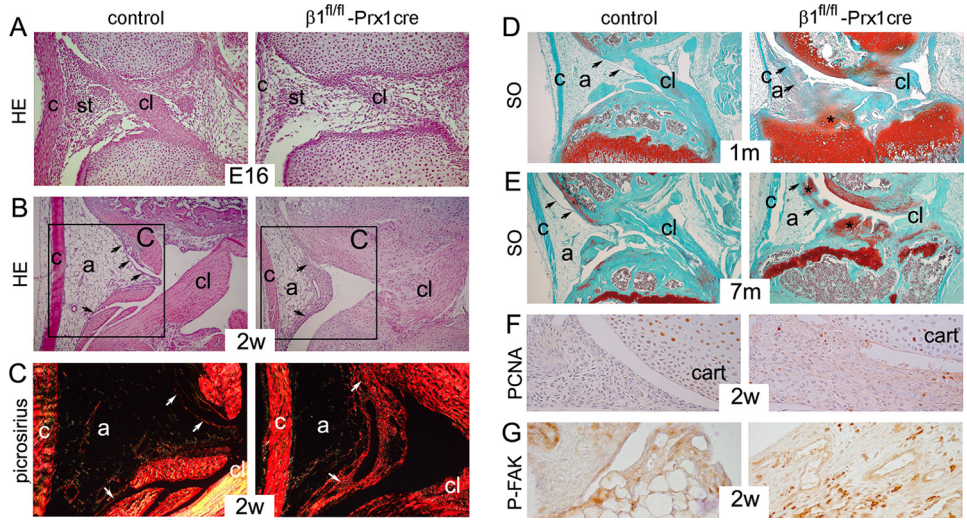

FIGURE 9. **Synovial abnormalities in $\beta1^{fl/fl}$-*Prx1cre*$^{+}$ mice.** *A* and *B*, photomicrographs of HE-stained midsagittal sections of the knee joints. *A*, looser appearance of the developing synovial tissue (*st*) and the delayed formation of the cruciate ligament (*cl*) were observed in 16-day-old mutant embryo (*E16*). Also note the thinner collateral ligament (*c*) in mutant. *B*, at 2 weeks (*2w*), the control synovium consists of a thin lining layer (*arrows*) and a large adipose (*a*) tissue. In mutant, the lining is hyperplastic with large vessels, and the amount of adipose tissue is reduced. *C*, picrosirius staining followed by polarization microscopy of the *boxed areas* in *B* reveals fibrosis of the mutant synovium, as shown by the strongly birefringent collagen deposits (*white arrows*). Also note the reduced birefringence in the mutant cruciate ligament, demonstrating structurally abnormal, less oriented, collagen fibrils in this tissue. *D* and *E*, photomicrographs of safranin orange-Fast green (*SO*)-stained sections. *D*, at 1 month, the intercondylar tibial surface is cartilaginous in the mutant and covered by the synovial tissue, showing signs of chondrification (*asterisk*). *E*, by 7 months, extensive chondrification (*asterisks*) is observed in the joint space and in the synovial lining (*arrows*) of mutant. *F*, increased numbers of PCNA-positive synovial cells are visible in the mutant. *G*, increased phosphorylation of FAK was evident in fibroblast-like cells of the mutant synovium. All stains were performed on paraffin sections, and the results are representative of those seen in at least four mice of each genotype at each age.

Histology of the knee joints revealed increased AC depth and a reduced ratio of uncalcified/calcified cartilage thicknesses in mutant mice compared with controls. This phenomenon might be the consequence of abnormal secondary ossification and subchondral bone formation. Since the articular cartilage and the underlying subchondral bone together provide the joint with its normal biomechanical properties, it is possible that the increased thickness of the calcified zone in mutant mice is due to a physiological compensation of the reduced subchondral bone mass to adopt mechanical loading. Supporting this hypothesis, it was recently reported that C57Bl/6 mice with a thin subchondral plate exhibit a higher calcified/uncalcified ratio in the AC than C3H/HEJ mice, which have a thick subchondral plate (32). At the molecular level, the increased calcified thickness of the $\beta1^{fl/fl}$-*Prx1cre*$^{+}$ AC was also apparent from the expression of collagen X, a hypertrophic chondrocyte marker that is normally deposited below the tidemark (1). Several previous studies have indicated an inductive role of β1 integrins in hypertrophic differentiation. Signaling via α1β1 and α5β1 integrins was required for hypertrophy of cultured AC chondrocytes induced by transglutaminases (33, 34), β1 integrin-blocking antibody impaired chondrocyte hypertrophy and collagen X deposition in sternal organ culture (35), and misexpression of α5β1 integrin in embryonic chick legs resulted in joint fusion and initiation of the hypertrophic differentiation program (13). Finally, we have demonstrated that hypertrophic differentiation is delayed in $\beta1^{fl/fl}$-*Col2cre*$^{+}$ growth plate and epiphyseal cartilages (10). Here we show that collagen X demarcates a broader calcified zone in $\beta1^{fl/fl}$-*Prx1cre*$^{+}$ knee joints and appears in cells above the tidemark, suggesting that β1 integrin signaling may actually prevent terminal differentiation of AC chondrocytes. This implies that integrins have a complex role in chondrocyte hypertrophy, which obviously depends on the tissue context.

$\beta1^{fl/fl}$-*Prx1cre*$^{+}$ AC displays several abnormalities, which are reminiscent of those found previously in the growth plate of the $\beta1^{fl/fl}$-*Col2a1cre* mice (10). In the normal growth plate, chon-

DISCUSSION

Previous *in vivo* studies in mice revealed that the loss of β1 integrins on chondrocytes results in severe growth plate defects and perinatal lethality (10), whereas ablation of the α1β1 integrin leads to accelerated knee OA (25). Here we report the generation of $\beta1^{fl/fl}$-*Prx1cre*$^{+}$ mice and demonstrate that targeting β1 integrin in limb skeletal precursor cells leads to a complex knee joint phenotype characterized by multiple AC and synovial abnormalities but is not accompanied by altered cartilage metabolism.

drocytes are flattened in the proliferative zone, where they arrange into distinct vertical columns (36), whereas in the normal AC, flat chondrocytes are apparent in the superficial zone, and column-like, vertical alignment of chondrocytes can be observed in the radial and calcified zones of the condyles (37). The growth plate of $\beta1^{fl/fl}$-*Col2a1cre* mice has rounded proliferative chondrocytes that are unable to form vertical columns due to a migratory block following cytokinesis (10). Similarly, $\beta1^{fl/fl}$-*Prx1cre*$^{+}$ chondrocytes were rounded in the superficial zone and were not aligned into columns in deeper regions, resulting in a more isotropic cell distribution compared with the normal, structural anisotropy seen in the control AC. The inability of β1 integrin-deficient chondrocytes to form organized structures in cartilage can be explained by the impaired adhesion and by the disruption of the F-actin and the normal matrix architecture. It has been shown that administration of anti-β1 integrin-blocking antibody to chicken sternum organ culture disrupts the cortical actin network and reduces chondrocyte-matrix interactions, revealed by fewer collagen fibrils and filopodia-like cell projections in the PM (35). Interestingly, our electron microscopic analysis of $\beta1^{fl/fl}$-*Prx1cre*$^{+}$ AC revealed an enlarged PM compartment with unusually thick collagen fibrils closely associated with the plasma membrane and with a large number of long microvilli. The normal PM consists of proteins that bind to β1 integrins, such as collagens II, VI, and fibronectin (1, 6). The observation that β1 integrin deficiency results in abnormalities of the collagen II network and deposition of collagen VI suggests that β1 integrins are pivotal organizers of the collagenous architecture of the matrix. Defects in pericellular collagen assembly could directly affect the size of the compartment, leading to its expansion as observed around $\beta1^{fl/fl}$-*Prx1cre*$^{+}$ chondrocytes. The elongation of the cell processes is probably due to the altered pericellular environment, as suggested in a recent study demonstrating multiple, elongated microvilli in human OA femoral head cartilage (38).

Finally, both growth plate and AC β1-null chondrocytes exhibit proliferation defect, frequent binucleation, and increased apoptosis. Since the current view suggests that AC growth is primarily achieved by apposition from the surface (39), the depletion of proliferative chondrocytes in this region could be the primary cause of reduced cellularity seen in the $\beta1^{fl/fl}$-*Prx1cre*$^{+}$ mice. Binucleation, caused by cytokinesis failure, cell fusion, or amitosis, is relatively common in auricular and articular chondrocytes (40). Since β1 integrins are localized in the cleavage furrow (10) and adhesion-mediated pulling forces are required to separate daughter cells (41), it is likely that the high binucleation rate in β1-integrin-null chondrocytes is due to impaired cytokinesis. Interestingly, although the number of binucleated cells is significantly higher in mutant mice at each age (Fig. 5*D*), there is significant difference in the number of PCNA-positive articular chondrocytes between genotypes only at 2 weeks of age (Fig. 5*B*). We have previously observed a progressive proliferation defect in postnatal but not in embryonic β1 integrin-deficient growth plates (10). This may indicate that maturation of the cartilage matrix triggers and/or aggravates the proliferation phenotype of β1-null cells, resulting in an apparently normal PCNA index of AC chondrocytes around birth (less mature cartilage) and in an obviously decreased PCNA index at 2 weeks (more mature cartilage). From 1 month of age, AC chondrocytes barely proliferate (Fig. 5*B*), but although the few PCNA positive cells in controls have a single nucleus, the majority of PCNA-stained mutant cells are binucleated (not shown). We hypothesize that those binucleated mutant chondrocytes are arrested in the cell cycle and increase the PCNA index to a level comparable with that of the controls. $\beta1^{fl/fl}$-*Prx1cre*$^{+}$ AC also displays slightly elevated numbers of apoptotic chondrocytes at 7 months of age. Just like the proliferation defect, the cell death seems to be progressive, and it may be, at least partially, induced by mechanical stress, since 12-month-old mutant mice with reduced mobility display an apoptotic rate similar to that of control mice. Nevertheless, the lack of massive cell death in the mutant AC suggests that other integrins (*e.g.* αvβ3) or non-integrin surface receptors may also support cell survival and partially prevent chondrocyte apoptosis in the absence of β1 integrins.

Despite the AC abnormalities resulting in a high histopathology score of $\beta1^{fl/fl}$-*Prx1cre*$^{+}$ knee joints at each age (Fig. *3A*), histology and histochemistry did not indicate increased proteoglycan depletion (Fig. 2, *G* and *H*) and cartilage erosion (Fig. *3B*) in the mutant AC compared with control mice. Age-dependent, progressive cartilage degradation was observed in control mice at ages 4, 7, and 12 months. The cartilage erosion was more severe in male than in female mice, suggesting that gender-specific physical activities, such as fighting, might worsen AC destruction. Mutant mice exhibited erosion scores similar to that of the controls at 4 and 7 months of age, whereas at 12 months, they displayed a moderately lower median value of the erosion grade than control mice. Because many severely affected $\beta1^{fl/fl}$-*Prx1cre*$^{+}$ mice died between 8 and 12 months of age due to the vascular phenotype and the survivors were less mobile, we propose that 12-month-old mutants had relatively milder AC erosion due to the lack of physical activities, especially in male mice.

At the molecular level, these results were corroborated with the apparently normal expression of MMP and ADAMTS proteases and their degradation products in the mutants, implying that β1 integrins are dispensable for overall cartilage metabolism *in vivo*. Mice lacking the major, chondrocyte-specific collagen-binding integrin α10β1 have no obvious AC abnormalities (11), further supporting the view that β1 integrins are less important for cartilage homeostasis. However, these observations are in contrast with the phenotype of the α1β1 integrin-deficient mice that display precocious PG loss and severe cartilage lesions associated with increased immunostaining of MMP-2 and MMP-3 (25). In normal joints, α1 integrin expression is low, whereas in OA cartilage, α1 is significantly up-regulated (14), suggesting that this particular integrin heterodimer might be required for cartilage matrix remodeling at the damaged regions. Our findings, however, clearly show that the loss of all β1 heterodimers on chondrocytes does not phenocopy the AC abnormalities of the α1-null mice. Could this contradiction be attributed to the abnormal gait and reduced mobility of $\beta1^{fl/fl}$-*Prx1cre*$^{+}$ mice? The fact that we did not notice significantly reduced mobility of mutant mice until 8 months of age, whereas α1 knock-out mice develop severe AC degeneration as

early as 4 months, argues against the possibility that reduced joint usage would prevent physical activity-induced cartilage damage in $\beta1^{fl/fl}$-*Prx1cre*$^{+}$ mice. Alternatively, the lack of β1 integrin heterodimers may attenuate AC destruction. Several studies indicate that integrins are involved in the regulation of MMPs expression in response to matrix degradation fragments in AC chondrocytes. First, the 110–140-kDa cell-binding and the 29-kDa, amino-terminal heparin-binding FN-fs are both capable of interacting with α5β1 integrin and up-regulate MMP-3 and/or MMP-13 via activation of the ERK1/2, p38, and JNK MAPKs (18, 20). Second, engagement of α2β1 or α5β1 integrins by adhesion-blocking antibodies on human AC chondrocytes increases ERK1/2, p38, and JNK phosphorylation, and blocking antibody to α5β1 stimulates gelatinase production (22). These studies implicate β1 integrins, particularly α2β1 and α5β1, as active participants in matrix degradation, and their absence may lower MMPs expression. However, the phosphorylation of MAPKs was apparently indistinguishable between $\beta1^{fl/fl}$-*Prx1cre*$^{+}$ and control ACs, indicating that either β1 integrins are not required for MAPK activation *per se*, or their lack can be efficiently compensated via signaling through β3/β5 integrins or growth factor receptors. More surprisingly, we found that FNIII7-10 fragments in explant culture were able to activate ERK and up-regulate MMP-13 expression in both control and β1 integrin-deficient femoral heads. Since not only α5β1 but also αvβ3 and αvβ5 integrins are capable of binding FNIII7-10 (42), it is likely that FN-f-induced cartilage degradation is a complex process involving signaling through several integrin heterodimers.

Synovial changes, including hyperplasia and inflammation, are often characteristics of OA joints and, via production of various cytokines and proteinases, synovitis probably contributes to cartilage destruction (43). $\beta1^{fl/fl}$-*Prx1cre*$^{+}$ mice display synovial fibrosis accompanied by frequent chondrification, but the mutant synovial tissue shows no clear sign of inflammatory infiltrates, suggesting that the observed alterations are unlikely to be linked to immunological processes. Recent findings indicate that synovial lining cells in OA patients display enhanced activation of FAK (44) that may lead to increased cell proliferation and/or migration. Indeed, and in contrast to chondrocytes, we detected up-regulation of phospho-FAK expression in mutant synovial tissue. Since FAK is tyrosine-phosphorylated in response to αvβ3 integrin ligation in osteoclasts (45), it is tempting to speculate that β1-deficient synovial fibroblasts may overuse αvβ3-mediated signaling pathways, resulting in altered FAK activation. However, the precise mechanism of how altered cell-matrix interactions and integrin signaling contribute to the synovial pathology of $\beta1^{fl/fl}$-*Prx1cre*$^{+}$ mice remains to be elucidated. Finally, interarticular ligaments were severely affected in the mutants, which might also contribute to the general pathology of the knee joint. We cannot exclude the possibility that joint instability caused by intra- and/or extra-articular ligament abnormalities leads to secondary effects in the knee AC; however, other joints (*e.g.* the tibiotalar joint of the ankle) that lack intrinsic ligaments exhibit similar AC defects (not shown) in $\beta1^{fl/fl}$-*Prx1cre*$^{+}$ mice.

Taken together, our study indicates that β1 integrins are pivotal for joint development regulating structural organization, differentiation, and growth of the AC and the synovium. The lack of β1 integrins in the AC, however, has no obvious impact on cartilage homeostasis, excluding β1-integrin signaling as a good candidate for intervention in degenerative cartilage diseases. Due to the complex phenotype of $\beta1^{fl/fl}$-*Prx1cre*$^{+}$ joints, however, the generation of a transgenic line with AC-specific deletion is required to precisely define the role of β1 integrin-mediated chondrocyte-ECM interactions in AC destruction.

Acknowledgments—We thank Zsuzsanna Farkas, Jannine Wagner, and Hildegard Reiter for excellent technical assistance.

REFERENCES

1. Poole, A. R., Kojima, T., Yasuda, T., Mwale, F., Kobayashi, M., and Laverty, S. (2001) *Clin. Orthop. Relat. Res.* **391,** S26–S33
2. Caterson, B., Flannery, C. R., Hughes, C. E., and Little, C. B. (2000) *Matrix Biol.* **19,** 333–344
3. Poole, A. R., Nelson, F., Dahlberg, L., Tchetina, E., Kobayashi, M., Yasuda, T., Laverty, S., Squires, G., Kojima, T., Wu, W., and Billinghurst, R. C. (2003) *Biochem. Soc. Symp.* **70,** 115–123
4. Jones, G. C., and Riley, G. P. (2005) *Arthritis Res. Ther.* **7,** 160–169
5. Murphy, G., Knäuper, V., Atkinson, S., Butler, G., English, W., Hutton, M., Stracke, J., and Clark, I. (2002) *Arthritis Res.* **4,** S39–S49
6. Knudson, W., and Loeser, R. F. (2002) *Cell Mol. Life Sci.* **59,** 36–44
7. Brakebusch, C., Bouvard, D., Stanchi, F., Sakai, T., and Fässler, R. (2002) *J. Clin. Invest.* **109,** 999–1006
8. Hynes, R. O. (2002) *Cell* **110,** 673–687
9. Loeser, R. F. (2000) *Biorheology* **37,** 109–116
10. Aszodi, A., Hunziker, E. B., Brakebusch, C., and Fässler, R. (2003) *Genes Dev.* **17,** 2465–2479
11. Bengtsson, T., Aszodi, A., Nicolae, C., Hunziker, E. B., Lundgren-Akerlund, E., and Fässler, R. (2005) *J. Cell Sci.* **118,** 929–936
12. Grashoff, C., Aszódi, A., Sakai, T., Hunziker, E. B., and Fässler, R. (2003) *EMBO Rep.* **4,** 432–438
13. Garciadiego-Cázares, D., Rosales, C., Katoh, M., and Chimal-Monroy, J. (2004) *Development* **131,** 4735–4742
14. Loeser, R. F., Carlson, C. S., and McGee, M. P. (1995) *Exp. Cell Res.* **217,** 248–257
15. Lapadula, G., Iannone, F., Zuccaro, C., Grattagliano, V., Covelli, M., Patella, V., Lo Bianco, G., and Pipitone, V. (1998) *Clin. Rheumatol.* **17,** 99–104
16. Ostergaard, K., Salter, D. M., Petersen, J., Bendtzen, K., Hvolris, J., and Andersen, C. B. (1998) *Ann. Rheum. Dis.* **57,** 303–308
17. Pulai, J. I., Del Carlo, M., Jr., and Loeser, R. F. (2002) *Arthritis Rheum.* **46,** 1528–1535
18. Ding, L., Guo, D., and Homandberg, G. A. (2008) *Osteoarthritis Cartilage* **16,** 1253–1262
19. Homandberg, G. A., Meyers, R., and Xie, D. L. (1992) *J. Biol. Chem.* **267,** 3597–3604
20. Stanton, H., Ung, L., and Fosang, A. J. (2002) *Biochem. J.* **364,** 181–190
21. Xie, D. L., Hui, F., Meyers, R., and Homandberg, G. A. (1994) *Arch. Biochem. Biophys.* **311,** 205–212
22. Forsyth, C. B., Pulai, J., and Loeser, R. F. (2002) *Arthritis Rheum.* **46,** 2368–2376
23. Loeser, R. F., Forsyth, C. B., Samarel, A. M., and Im, H. J. (2003) *J. Biol. Chem.* **278,** 24577–24585
24. Werb, Z., Tremble, P. M., Behrendtsen, O., Crowley, E., and Damsky, C. H. (1989) *J. Cell Biol.* **109,** 877–889
25. Zemmyo, M., Meharra, E. J., Kühn, K., Creighton-Achermann, L., and Lotz, M. (2003) *Arthritis Rheum.* **48,** 2873–2880
26. Logan, M., Martin, J. F., Nagy, A., Lobe, C., Olson, E. N., and Tabin, C. J. (2002) *Genesis* **33,** 77–80
27. Potocnik, A. J., Brakebusch, C., and Fässler, R. (2000) *Immunity* **12,** 653–663
28. Modis, L. (1991) *Organization of the Extracellular Matrix: A Polarization*

Microscopic Approach, p. 269, CRC Press, Inc., Boca Raton, FL
29. Sakai, K., Hiripi, L., Glumoff, V., Brandau, O., Eerola, R., Vuorio, E., Bösze, Z., Fässler, R., and Aszódi, A. (2001) *Matrix Biol.* **19,** 761–767
30. Aszódi, A., Chan, D., Hunziker, E., Bateman, J. F., and Fässler, R. (1998) *J. Cell Biol.* **143,** 1399–1412
31. Loeser, R. F., Erickson, E. A., and Long, D. L. (2008) *Curr. Opin. Rheumatol.* **20,** 581–586
32. Botter, S. M., van Osch, G. J., Waarsing, J. H., van der Linden, J. C., Verhaar, J. A., Pols, H. A., van Leeuwen, J. P., and Weinans, H. (2008) *Osteoarthritis Cartilage* **16,** 506–514
33. Johnson, K. A., Rose, D. M., and Terkeltaub, R. A. (2008) *J. Cell Sci.* **121,** 2256–2264
34. Tanaka, K., Yokosaki, Y., Higashikawa, F., Saito, Y., Eboshida, A., and Ochi, M. (2007) *Matrix Biol.* **26,** 409–418
35. Hirsch, M. S., Lunsford, L. E., Trinkaus-Randall, V., and Svoboda, K. K. (1997) *Dev. Dyn.* **210,** 249–263
36. Erlebacher, A., Filvaroff, E. H., Gitelman, S. E., and Derynck, R. (1995) *Cell* **80,** 371–378
37. Hunziker, E. (1992) *Articular Cartilage and Osteoarthritis* (Kuettner, K. E., ed) pp. 183–199, Raven Press, New York
38. Holloway, I., Kayser, M., Lee, D. A., Bader, D. L., Bentley, G., and Knight, M. M. (2004) *Osteoarthritis Cartilage* **12,** 17–24
39. Dowthwaite, G. P., Bishop, J. C., Redman, S. N., Khan, I. M., Rooney, P., Evans, D. J., Haughton, L., Bayram, Z., Boyer, S., Thomson, B., Wolfe, M. S., and Archer, C. W. (2004) *J. Cell Sci.* **117,** 889–897
40. Lipman, J. M., Hicks, B. J., and Sokoloff, L. (1984) *Experientia* **40,** 553–554
41. Böttcher, R. T., Wiesner, S., Braun, A., Wimmer, R., Berna, A., Elad, N., Medalia, O., Pfeifer, A., Aszódi, A., Costell, M., and Fässler, R. (2009) *EMBO J.* **28,** 1157–1169
42. Leiss, M., Beckmann, K., Girós, A., Costell, M., and Fässler, R. (2008) *Curr. Opin. Cell Biol.* **20,** 502–507
43. Goldring, M. B., and Goldring, S. R. (2007) *J. Cell Physiol.* **213,** 626–634
44. Shahrara, S., Castro-Rueda, H. P., Haines, G. K., and Koch, A. E. (2007) *Arthritis Res. Ther.* **9,** R112
45. Chen, H. C., and Guan, J. L. (1994) *Proc. Natl. Acad. Sci. U.S.A.* **91,** 10148–10152